

# Constraining Lorentz invariance violations using the Crab pulsar TeV emission

---

**Markus Gaug\***

*Unitat de Física de les Radiacions, Departament de Física, and CERES-IEEC, Universitat Autònoma de Barcelona, E-08193 Bellaterra, Spain*

*E-mail: [markus.gaug@uab.cat](mailto:markus.gaug@uab.cat)*

**Daniel Garrido**

*Unitat de Física de les Radiacions, Departament de Física, and CERES-IEEC, Universitat Autònoma de Barcelona, E-08193 Bellaterra, Spain*

*E-mail: [daniel.garrido@uab.cat](mailto:daniel.garrido@uab.cat)*

Fast variations of gamma-ray flux from Active Galactic Nuclei and Gamma-Ray Bursts can constrain Lorentz Invariance Violation (LIV) because of the delayed (or advanced) arrival of photons with higher energies: this approach has led to the current world-best limits on the energy scale of Quantum Gravity. Here we report on constraints on LIV studying the gamma-ray emission up to TeV energies from the Galactic Crab pulsar, recently discovered by the MAGIC collaboration. A likelihood analysis of the pulsar events reconstructed for energies above 400 GeV finds no significant variation of energy-dependent arrival time, and 95% CL limits are then obtained on the effective LIV energy scale after taking into account systematic uncertainties. Only a factor of about two less constraining than the current world-best limit on a quadratic LIV scenario, pulsars are now well established as a third and independent class of astrophysical objects suitable to constrain the characteristic energy scale of LIV.

*35th International Cosmic Ray Conference - ICRC217-  
10-20 July, 2017  
Bexco, Busan, Korea*

---

\*Speaker.

## 1. Introduction

Quantum Gravity (QG) models [1] combine the field equations of general relativity with quantum field theory. Many such scenarios include spontaneous violation of the Lorentz invariance (LIV) [2, 3, 4, 5, 6, 7, 8], which lead, among others, to energy dependent dispersion relations of the photon in vacuum. While such effects are expected to become important at energies of the order of the Planck scale ( $E_{Pl} = \sqrt{\hbar c^5/G} \approx 1.22 \cdot 10^{19}$  GeV), they can manifest themselves already at much lower energies, through tiny deviations from the Lorentz invariant scenario, which accumulate once the photons travel very large distances [9]. Introducing an effective quantum gravity scale  $E_{QG_n}$ , which may be of the order of the Planck energy or lower, the group velocity of photons of energy  $E \ll E_{QG_n}$  can be expressed as an expansion in powers of  $E$  (see e.g. [9]), where:

$$u_\gamma(E) = \frac{\partial E}{\partial p} \approx c \cdot \left[ 1 - \xi_n \frac{n+1}{2} \left( \frac{E}{E_{QG_n}} \right)^n \right]. \quad (1.1)$$

Here,  $\xi_n = +1$  stands for a subluminal scenario, while  $\xi_n = -1$  characterizes a superluminal scenario, and  $\xi_n = 0$  for the case that the corresponding order is forbidden<sup>1</sup>. We consider here terms with  $n > 0$ , which produce energy dependent velocities, typically considered in time-of-flight experiments, and there the linear case of  $n = 1$  and the quadratic case  $n = 2$ . Odd terms of  $n$  violate *CPT* [11], that's why the  $n = 2$  case may dominate if *CPT* is conserved.

Energy-dependent arrival time variations have been studied so far using flares from Active Galactic Nuclei (AGNs) [12, 13], and the very fast flux variations of Gamma-ray bursts (GRBs) [14, 15]. The latter have achieved sensitivities to the linear case  $E_{QG_1}$  of well beyond the Planck scale [14, 16] which has been effectively excluded. Constraints on  $E_{QG_1}$  have been obtained from the Crab pulsar starting from 1969 already [17] and constantly improved since then [18, 19]. Although the Crab pulsar is found many orders of magnitude closer to us than AGNs and GRBs, some of them observed at cosmological distances, its pulsations repeat and can be added over many periods to improve sensitivity to LIV.

## 2. MAGIC observation of TeV emission from the Crab Pulsar

The Major Atmospheric Gamma-ray Imaging Cherenkov system (MAGIC) is located at the Roque de los Muchachos observatory (28.8°N, 17.8°W, 2200 m a.s.l.), in the Canary Island of La Palma, Spain. The MAGIC system consisted of a single 17 m-dish telescope during its first 5 years of operation [20] to which, in 2009, a second telescope was added in order to create a stereo system [21]. A major upgrade was carried out between 2011 and 2012 [22, 23].

The Crab Nebula, together with its Pulsar, which cannot be spatially separated so far by Imaging Atmospheric Cherenkov Telescopes (IACTs), has been observed by MAGIC in every possible hardware configuration since its start. Being the brightest steady Very High Energy (VHE) gamma-ray source in the sky, it is regularly observed for calibration purposes and performance monitoring, leading to more than thousand hours of total observation time. These data have been down-selected

<sup>1</sup>Eq. 1.1 neglects terms breaking rotation invariance which if there, would however imply some breaking of boost invariance as well [10]

to slightly more than 300 h of excellent quality, including single telescope (“mono”) and dual telescope (“stereo”) configurations, and requiring simultaneous precision time stamping which allows to attribute a precise pulsar phase value to each registered event, using ephemerides provided by the Jodrell Bank Observatory [24].

With these data, MAGIC has detected emission from the Crab Pulsar up to 0.5 TeV for the main pulse  $P1$ , and up to 1.5 TeV for the inter-pulse  $P2$  [25], showing  $544 \pm 92$  excess events for  $P2$  above 400 GeV. The spectrum of both pulses is consistent with a power-law, however a significant difference was found between the reconstructed spectral indices of  $P1$  and  $P2$ , the latter being harder [25]. This unique set of data is now used to test LIV.

### 3. Maximum likelihood method

We construct a maximum likelihood method following the approach of [26], further elaborated in [13, 14], and slightly adapted for the quadratic LIV effect. Two new parameters are defined:  $\lambda_1 \equiv 10^{19} \text{ GeV}/E_{QG_1}$  and  $\lambda_2 \equiv 10^{12} \text{ GeV}/E_{QG_2}$ . The LIV effect under test (Eq. 1.1) produces then a mean phase delay of<sup>2</sup>:

$$\Delta\phi_n = c_n \cdot \left( \lambda_n \cdot \left( \frac{E}{\text{GeV}} \right) \right)^n, \quad (3.1)$$

with :

$$c_1 = \xi_1 \cdot \frac{d_{\text{Crab}}}{c \cdot P_{\text{Crab}}} \cdot 10^{-19} \quad (\text{GeV}^{-1}) \quad (3.2)$$

$$c_2 = \xi_2 \cdot \frac{3}{2} \frac{d_{\text{Crab}}}{c \cdot P_{\text{Crab}}} \cdot 10^{-24} \quad (\text{GeV}^{-2}), \quad (3.3)$$

where  $d_{\text{Crab}}$  is the pulsar distance,  $c$  the Lorentz-invariant speed of light,  $P_{\text{Crab}}$  the pulsar period.

We use now the profile likelihood ratio method [27] to define a test statistic  $D_n$ :

$$D_n(\lambda_n | \mathbf{X}) = -2 \ln \left( \frac{\mathcal{L}(\lambda_n; \hat{\mathbf{v}}(\lambda_n) | \mathbf{X})}{\mathcal{L}(\hat{\lambda}_n; \hat{\mathbf{v}} | \mathbf{X})} \right). \quad (3.4)$$

of our pulsar dataset  $\mathbf{X} = \{E'_i, \phi'_i, k_i\}$  and a set of nuisance parameters  $\mathbf{v}$ . Here,  $E'_i$  is the reconstructed energy of each event  $i$ ,  $\phi'_i$  its reconstructed phase and  $k_i$  the observation period. Single-hatted parameters  $\{\hat{\lambda}_n, \hat{\mathbf{v}}\}$  maximize the likelihood, while double-hatted parameters  $\hat{\hat{\mathbf{v}}}$  are those that maximize  $\mathcal{L}$  under the assumption of  $\lambda_n$ .

<sup>2</sup>The definition of  $\lambda_2$  differs slightly from [13, 14], which is now directly proportional to  $1/E_{QG_2}$  (the quantity of interest), instead of  $1/E_{QG_2}^2$ .

The likelihood  $\mathcal{L}$  takes the form of an *extended likelihood* [29]:

$$\mathcal{L}(\lambda_n; \mathbf{v} | \mathbf{X}) = \mathcal{L}(\lambda_n; f, \alpha, \phi_{P2}, \sigma_{P2} | \{ \{ E'_i, \phi'_i \}_{i=0}^{N_k} \}_{k=0}^{N_s}) \quad (3.5)$$

$$\begin{aligned} &= P(\mathbf{v}) \cdot \prod_{k=0}^{N_s} \exp \left( -g_k(\lambda_n; \mathbf{v}) - b_k \cdot \frac{1+\tau}{\tau} \right) \cdot \prod_{m=0}^{N_k^{OFF}} b_k \cdot \\ &\quad \cdot \prod_{i=0}^{N_k^{ON}} (g_k(\lambda_n; \mathbf{v}) + b_k/\tau) \cdot \mathcal{P}_k(E'_i, \phi'_i | \lambda_n; \mathbf{v}) . \end{aligned} \quad (3.6)$$

Here,  $N_s$  denotes the number of observation periods,  $N_k^{ON}$  and  $N_k^{OFF}$  the number of events in the  $P2$   $ON$  pulse region and the background control  $OFF$  regions for observation period  $k$ , while  $g_k$  and  $b_k$  are their expectation values, respectively. We used  $\phi' \in [0.3558, 0.4495]$  to define the  $ON$  region (optimized through simulations),  $\phi' \in [0.52, 0.87]$  [30] for the  $OFF$  region, and  $E' \in [0.4, 7]$  TeV. This choice for the  $ON$  region excludes contributions of  $P1$  and practically all possible contributions from bridge emission [31]. unnecessarily complicating the PDF and adding systematic uncertainties to the results. The ratio of phase width of the  $OFF$ , divided by the one of the  $ON$  region is labelled  $\tau$ . The background expectation values  $b_k$  are direct nuisance parameters, while the signal expectation contains the flux normalization  $f$  as nuisance parameter. A possible probability density function (PDF) for the nuisance parameters, known from external measurements, is labelled  $P(\mathbf{v})$ . The set of nuisance parameters contains, apart from the  $b_k$ : the  $P2$  flux normalization  $f$ , its spectral index  $\alpha$ , the mean pulse position  $\phi_{P2}$  and its width  $\sigma_{P2}$ <sup>3</sup>.

The PDF of event  $i$  is a combination of PDFs for signal (a pulsar event:  $S_k(E'_i, \phi'_i | \lambda_n; \mathbf{v})$ ), or the (interpolated) spectral energy distribution of the background:  $h_k(E'_i)$  (see e.g. [32]), for the  $k$ -th data subsample, respectively:

$$\mathcal{P}_k(E'_i, \phi'_i | \lambda_n; \mathbf{v}) = \frac{b_k/\tau \cdot h_k(E'_i) + g_k(\lambda_n; \mathbf{v}) \cdot S_k(E'_i, \phi'_i | \lambda_n; \mathbf{v})}{g_k(\lambda_n; \mathbf{v}) + b_k/\tau} . \quad (3.7)$$

The normalization constants of  $S_k$  and  $h_k$ , and later  $g_k$  and  $b_k$ , depend on all nuisance parameters and on  $\lambda_n$ . The signal PDF,  $S_k(E'_i, \phi'_i | \lambda_n; \mathbf{v})$ , is written as:

$$S_k(E'_i, \phi'_i | \lambda_n; \mathbf{v}) = \frac{\Delta t_k \int_0^\infty R_k(E | E'_i) \cdot \Gamma_{P2}(E, f, \alpha) \cdot F_{P2}(\phi'_i, E | \lambda_n; \phi_{P2}, \sigma_{P2}) dE}{g_k(\lambda_n; \mathbf{v})} . \quad (3.8)$$

Here,  $\Delta t_k$  denotes the effective observation time for each  $k$ -th data subsample,  $R_k$  the product of the effective collection area and the (inverted) energy re-distribution function to obtain a photon of true energy  $E$ , given its reconstructed energy  $E'$ , both obtained from Monte-Carlo simulations. The  $P2$  pulsar spectrum  $\Gamma_{P2}$  has been chosen to:

$$\Gamma_{P2}(E) = f \cdot (E/E_{dec})^{-\alpha} \cdot \exp(-E/E_b) \quad \text{TeV}^{-1} \text{cm}^{-2} \text{s}^{-1} , \quad (3.9)$$

according to the findings of [25]<sup>4</sup>. The pulsar phaseogram model  $F_{P2}$  is computed as:

$$F_{P2}(\phi'_i, E | \lambda_n; \phi_{P2}, \sigma_{P2}) = \frac{1}{\sqrt{2\pi}\sigma_{P2}} \cdot \exp \left[ -\frac{\left( \phi'_i - \phi_{P2} - \Delta\phi(E | \lambda_n) \right)^2}{2\sigma_{P2}^2} \right] , \quad (3.10)$$

<sup>3</sup>Nuisance parameters might also include additional asymmetry parameters, a spectral cutoff or other variables parameterizing a different pulse model.

<sup>4</sup>[25] excludes a possible spectral cutoff below 700 GeV.

where the observed width  $\sigma_{p2}$  contains contributions of the intrinsic pulse width and the instrumental phase resolution, both considered Gaussian in nature<sup>5</sup>, and  $\Delta\phi$  denotes the hypothetical phase delay produced by LIV, Eq. 3.1.

#### 4. Results

The profile likelihood algorithm Eq. 3.4 has been applied to the MAGIC Crab Pulsar data set [25], using the *TMinuit* class of *ROOT* [33] for the minimization. The minima of the profile likelihood were found close to zero in all cases (see Fig. 1). Table 1 displays the nuisance parameters obtained at the minimum, all compatible with those obtained in [25].

nuisance parameter	result	unit
$\hat{f}$	$6.3 \pm 0.7$	$(\cdot 10^{-10} \text{ TeV}^{-1} \text{ cm}^{-2} \text{ s}^{-1})$
$\hat{\alpha}$	$2.81 \pm 0.07$	1
$\hat{\phi}_{p2}$	$0.403 \pm 0.003$	1
$\hat{\sigma}_{p2}$	$0.015 \pm 0.003$	1

**Table 1:** Nuisance parameter values at the minima of  $\lambda_{1,2}$ . Uncertainties are statistical only, obtained from the diagonal elements of the covariance matrix, provided by *TMinuit*.

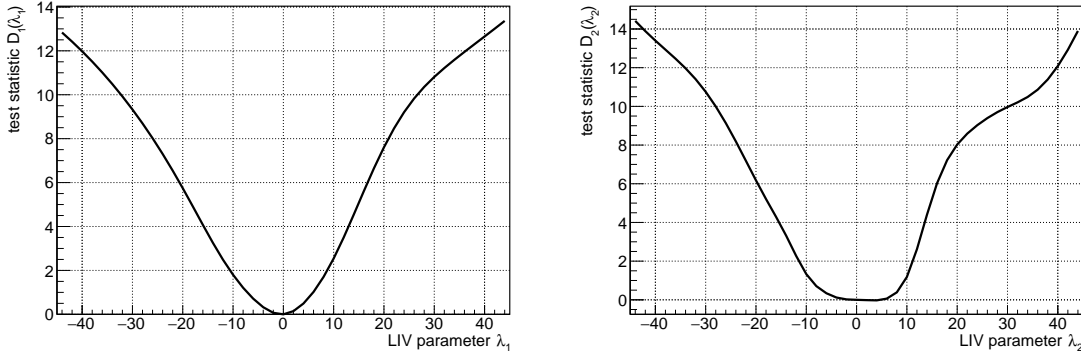


**Figure 1:** Left: test statistic (Eq. 3.4) as a function of  $\lambda_1$ , right: as a function of  $\lambda_2$ .

#### 5. Discussion and Conclusions

95% confidence limits (CL) limits have been obtained by evaluating the likelihood at  $\tilde{D}_n = \Delta\tilde{D}_n^{95\%}$ , where  $\Delta\tilde{D}_n^{95\%}$  has been obtained from simulations and found slightly higher than the canonical value of  $\Delta\tilde{D}_n^{95\%} = 2.705$  [28]. The difference is due to the nuisance parameters which have been varied in the simulations, using the covariance matrix obtained from the likelihood applied to experimental data.

<sup>5</sup>An intrinsic Lorentzian pulse shape has been investigated as well, yielding similar results.

We studied systematic effects due to the insufficient knowledge, i.e. modelling of the likelihood, with respect to the background estimation, possible shifts in the assumed scale for energy and flux, different pulse shapes, including asymmetric behaviour, different values for the cutoff energy  $E_b$ , possible residual contributions from bridge emission and the uncertainty of the pulsar distance. All values add up quadratically to about 42% for the linear case, and 36% for the quadratic one, respectively. It should be admitted here however, that energy dependent source-intrinsic effects might be possible and require further attention in the future.

Table 2 shows the obtained limits, with and without systematic uncertainties.

case	95% CL limit (w/o systematic)	95% CL limit (incl. systematics)
$\xi_1 = +1$	$E_{QG_1} > 7.8 \cdot 10^{17}$ GeV	$E_{QG_1} > 5.5 \cdot 10^{17}$ GeV
$\xi_1 = -1$	$E_{QG_1} > 6.4 \cdot 10^{17}$ GeV	$E_{QG_1} > 4.5 \cdot 10^{17}$ GeV
$\xi_2 = +1$	$E_{QG_2} > 8.0 \cdot 10^{10}$ GeV	$E_{QG_2} > 5.9 \cdot 10^{10}$ GeV
$\xi_2 = -1$	$E_{QG_2} > 7.2 \cdot 10^{10}$ GeV	$E_{QG_2} > 5.3 \cdot 10^{10}$ GeV

**Table 2:** Obtained limits applying the profile likelihood method.

These limits are found well below experimental results obtained on GRBs [14] and hence not competitive for the linear case. The quadratic case yields, however, constraints only about a factor two from the current best limits [14]. Since there are currently strong arguments against linear LIV effects, even suppressed by the Planck energy [34, 16], limits constraining the quadratic case are now of greater interest.

Pulsar data has the advantage that it can be continuously accumulated and sensitivity to LIV improved. MAGIC is currently at the zenith of its performance [23], which gives the possibility to take regular data on the Crab Pulsar, particularly at higher zenith angles where sensitivity for TeV energy gamma-rays is better. We expect that a data set of 2000 hours of stereo data, a number within reach for the MAGIC collaboration, can ensure an improvement of the quadratic limit by a factor of two, most probably even exceeding the current Fermi limit [14]. Moreover, our profile likelihood can be combined with that from other sources, like AGNs, or even other experiments. In such a way, significantly improved constraints on LIV are well within reach in the next years.

## Acknowledgments

We would like to thank the IAC for the excellent working conditions at the ORM in La Palma. We acknowledge the financial support of the German BMBF, DFG and MPG, the Italian INFN and INAF, the Swiss National Fund SNF, the European ERDF, the Spanish MINECO, the Japanese JSPS and MEXT, the Croatian CSF, and the Polish MNiSzW.

## References

- [1] Rovelli C. Quantum Gravity (Cambridge University Press), 2004.
- [2] Kostelecký V. A. & Samuel S. Phys. Rev. D, 39 (1989) 683.
- [3] Burgess C. P. et al., JHEP 3 (2002) 043.

- [4] Gambini R. & Pullin J., Phys. Rev. D 59 (1999), arXiv:gr-qc/9809038
- [5] Douglas M. R. & Nekrasov N. A. Rev. of Modern Phys. 73 (2001) 977.
- [6] Magueijo J. & Smolin L., Phys. Rev. Lett. 88 (2002) 190403.
- [7] Hamed-Arkani N. et al., JHEP 5 (2004) 074.
- [8] Hořava P., Phys. Rev. D 79 (2009) 084008.
- [9] Amelino-Camelia G. & Smolin L., Phys. Rev. D 80 (2009) 084017.
- [10] Mattingly D., Living Reviews in Relativity 8 (2005) 5.
- [11] Colladay D. & Kostelecký V. A., Phys. Rev. D 58 (1998) 116002.
- [12] Albert J. et al., Phys. Lett. B 668 (2008) 253.
- [13] Abramowski A. et al., Astrop. Phys. 34 (2011) 738.
- [14] Vasileiou V. et al., Phys. Rev. D 87 (2013) 122001,
- [15] Amelino-Camelia G. et al., Nature 393 (1998) 763.
- [16] Götz D. et al., MNRAS 444 (2014) 2776.
- [17] Warner B. & Nather R. E., Nature 222 (1969) 157.
- [18] Kaaret P., A&A 345 (1999) L32.
- [19] Otte N. in 32<sup>nd</sup> ICRC, Beijing, China (2011) Vol. 7, 256.
- [20] Cortina J., Goebel F. & Schweizer T. for the MAGIC Collaboration, in 31<sup>st</sup> ICRC, Lodz, Poland (2009). <http://arxiv.org/abs/0907.1211>
- [21] Aleksić J., et al., Astrop. Phys. 35 (2012) 435.
- [22] Aleksić J. et al., Astrop. Phys. 72 (2016) 61.
- [23] Aleksić J. et al., Astrop. Phys. 72 (2016) 76.
- [24] Lyne A. & Roberts M., Jodrell Bank Crab Pulsar Monthly Ephemeris (2014) <http://www.jb.man.ac.uk/~pulsar/crab.html>.
- [25] Ansoldi S. et al., A&A 585 (2016) A133, arXiv:1510.07048
- [26] Martinez M. & Errando M. Astrop. Phys. 31 (2009) 226.
- [27] Murphy S. A., & van der Vaart A. W., J. Am. Stat. Ass. 95 (2000) 449.
- [28] Olive K. & Particle Data Group, Chin. Phys. C 38 (2014) 090001.
- [29] Barlow R., NIM A 297 (1990) 496.
- [30] Fierro J. M. et al., ApJ 494 (1998) 734.
- [31] Aleksić J. et al., A&A 565 (2014) L12.
- [32] Aleksić J. et al., JCAP 2 (2014) 008.
- [33] Brun R. & James F., TMinuit Class Reference, <https://root.cern.ch/root/html534/TMinuit.html>
- [34] Kislat F. & Krawczynski H., Phys. Rev. D 95 (2017) 083013.